MNRAS **000**, 1–12 (2016) Preprint 5 July 2016 Compiled using MNRAS LATEX style file v3.0

Accretion of pristine gas and dilution during the formation of multiple-population globular clusters

A. D'Ercole[1⋆], F. D'Antona[2], E. Vesperini[3]
[1] *INAF, Osservatorio Astronomico di Bologna, via Ranzani 1, I-40127 Bologna, Italy*
[2] *INAF, Osservatorio Astronomico di Roma, Via Frascati 33, I-00040 Monteporzio Catone (Roma), Italy*
[3] *Department of Astronomy, Indiana University, Swain West, 727 E. 3rd Street, IN 47405 Bloomington (USA)*

arXiv:1607.00951v1 [astro-ph.GA] 4 Jul 2016

Accepted XXX. Received YYY; in original form ZZZ

ABSTRACT

We study the interaction of the early spherical GC wind powered by Type II supernovae (SNe II) with the surrounding ambient medium consisting of the gaseous disk of a star forming galaxy at redshift $z \gtrsim 2$. The bubble formed by the wind eventually breaks out of the disk, and most of the wind moves directly out of the galaxy and is definitively lost. The fraction of the wind moving nearly parallel to the galactic plane carves a hole in the disk which will contract after the end of the SN activity. During the interval of time between the end of the SN explosions and the "closure" of the hole, very O-poor stars (the Extreme population) can form out of the super–AGB (asymptotic giant branch) ejecta collected in the GC center. Once the hole contracts, the AGB ejecta mix with the pristine gas, allowing the formation of stars with an oxygen abundance intermediate between that of the very O-poor stars and that of the pristine gas. We show that this mechanism may explain why Extreme populations are present only in massive clusters, and can also produce a correlation between the spread in helium and the cluster mass.

Finally, we also explore the possibility that our proposed mechanism can be extended to the case of multiple populations showing bimodality in the iron content, with the presence of two populations characterized by a small difference in [Fe/H]. Such a result can be obtained taking into account the contribution of delayed SN II.

Key words: hydrodynamics – globular clusters: general – stars: chemically peculiar

1 INTRODUCTION

Many spectroscopic, spectrophotometric and photometric observational studies have revealed that globular clusters (GCs) host multiple stellar populations characterized by different chemical properties. While the first stellar generation (FG) has a chemical composition equal to that of the pristine gas, the second generation (SG) is depleted in C and O, enhanced in N and Na, and in some cases is also characterized by significant differences in helium; with few exceptions, the iron abundance is the same in all the stellar populations, indicating that the ejecta of the Type II supernovae (SNe II) belonging to the FG has been lost by the GC before the formation of the stellar SG (Piotto et al. 2015, and references therein) which otherwise should be very likely Fe-enhanced, at odd with what observed in most of the clusters.

In order to explain the picture provided by observational studies, a number of theoretical frameworks differing in the FG sources of the processed material out of which the SG forms have ben proposed: fast-rotating massive stars (Krause et al. 2013), massive interacting binaries (de Mink et al. 2009; Bastian et al. 2013), asymptotic giant branch (AGB) and super-AGB stars (D'Ercole et al. 2008, 2010). Despite the numerous theoretical efforts, many questions remain unanswered as none of the proposed scenarios is exempt from problems and some arbitrary assumptions.r

All the proposed models require the processed ejecta of the FG sources to be mixed and diluted with gas with pristine chemical composition. In this paper we focus on the dynamics of the dilution in the context of the AGB scenario, which has been originally proposed by D'Ercole et al. (2008) to account for the three populations, characterized by three different helium abundances, discovered in NGC 2808. According to this scenario, the GC is initially composed by FG stars with the chemical abundances of the pristine gas out of which they formed; subsequently, the SN II explosions clear the cluster of the remaining gas, and the super-AGB and AGB ejecta can collect in the cluster centre through a cooling flow; the stars created within this cooling flow form the SG population. In order to reproduce the observed Na-O an-

⋆ E-mail: annibale.dercole@oabo.inaf.it

© 2016 The Authors

ticorrelation it is however necessary to mix pristine gas with the AGB ejecta (see D'Ercole et al. 2010, 2011, 2012). In this framework, the only stars forming from pure AGB ejecta would be the very O-poor stars classified as Extreme (E) by Carretta et al. (2010) while stars with less extreme O depletion (those classified as Intermediate (I) by Carretta et al. (2010)) would form from a mix of ejecta and pristine gas. For clusters hosting E SG stars, dilution should start after the beginning of the formation of the SG while in clusters where the E population is absent SG formation should involve both AGB ejecta and pristine gas.

Renzini et al. (2015) have suggested that AGB models are far from having explored the entire parameter space, and a possible revision of the cross section of the reaction rate destroying sodium could lead to a reassessment of the need for the dilution. However, as already argued in D'Ercole et al. (2011), dilution with pristine gas is likely to remain as an essential ingredient also in the case a revision of AGB models were to lead to yields characterized by a Na-O anticorrelation.

Understanding the origin of this pristine gas and its dynamics during the early evolutionary stages of globular clusters and the phase of SG star formation is a key aspect in the study of multiple-population globular cluster formation. In this paper we present a model aimed at following the evolution of the gas within a globular cluster forming in the disk of a high-redshift galaxy. We are first guided by the idea of quantifying under which hypothesis the cluster gas may satisfy the simplest constraints for the formation of multiple populations, that is: *i*) initially the pristine gas must be completely removed, at least from the clusters displaying an extended Na-O anticorrelation (see above); *ii*) the cluster should be able to reaccrete the pristine gas about 20–30 Myr after the end of the SN II explosions[1]; *iii*) the pristine gas should not be contaminated by the SN II ejecta because in most clusters the different stellar populations have the same iron abundances

We find out that a model fulfilling these requirements is compatible with the formation of clusters in the disks of galaxies at $z > 2$ (see e.g. Kravtsov & Gnedin 2005; Kruijssen 2015, and references therein) and may also explain why extreme populations are present only in massive clusters. Interestingly, the model may be easily extended to the case of multiple populations showing bimodality in the iron content, with the presence of two (or more) populations differing in [Fe/H] by a generally small fraction. While the effects of the explosions of type II supernovae 'isolated in time' cannot be distinguished from the iron content of the clusters, which will be scarcely increased (D'Antona et al. 2016), we show that there may be cases in which delayed-SNII events may stop the cooling flow for a period of some decades of million years, but their energy output is not able to push the ejecta much beyond the cluster, allowing, at the end of this epoch, a new burst of star formation to occur in gas polluted by both supernovae ejecta and AGB ejecta.

[1] This time interval derives from the chemical models of D'Ercole et al. (2010, 2012).

2 SET-UP OF THE MODEL

The model follows the steps illustrated in Figure 1: (a) the globular cluster is assumed to form within the disk of a high-redshift galaxy (not necessarily in its nucleus, e.g. Kravtsov & Gnedin 2005; Bekki 2012); (b) the SNe II belonging to the FG start to explode powering a wind which drives a bubble; (c) the bubble eventually breaks out of the disk and the wind is almost all lost into the space surrounding the galaxy; (d) the hole in the disk carved by the wind expands to its maximum radius $R_{\rm st}$, when its expansion velocity decreases down to the local velocity dispersion σ_0 of the surrounding gas; (e) at the end of the SN activity the ambient matter then penetrates the cavity in a time of the order of $R_{\rm st}/\sigma_0$, and the disk gas, not affected by supernova contamination, dilutes the AGB ejecta out of which the SG Intermediate stars form.

In our simple model the disk is described by a stratified gas distribution characterized by its effective scale height

$$H_{\rm eff} = \frac{1}{\rho_0}\int_0^\infty \rho(z){\rm d}z, \qquad (1)$$

where ρ_0 is the density in the midplane. The pressure includes the turbulent pressure, and is defined as $P_0 = \rho_0\sigma_0^2$; this is a generalization of the thermal pressure because the total velocity dispersion is defined as $\sigma_0^2 = c_0^2+\upsilon_0^2$, where c_0 is the 1D thermal velocity dispersion and υ_0 the 1D turbulent velocity dispersion (e.g. Lequeux 2005). Koyama & Ostriker (2009) have shown that the inclusion of the contribution of the turbulence is necessary to support the common assumption that the interstellar medium of the Milky Way disk is in effective hydrostatic equilibrium. Moreover, the role of the turbulence prevails in star bursting galaxies like those where the GCs presumably formed , where the velocity dispersion might be as high as ~ 100 km s^{-1} (but see section 4).

We assume that the globular cluster is located in the midplane, and that its FG stars are characterized by a Kroupa (Kroupa 2001) initial mass function (IMF); the minimum mass of the SN II progenitors is $\rm M_{mass}$=8–9 $\rm M_\odot$, while the most massive exploding stars have $M = 20$ $\rm M_\odot$, as stars with higher masses may collapse quietly to black holes (Smartt 2009). Assuming that the FG forms in an instantaneous burst, the SN explosions are thus expected to last for a period $t_{\rm SN}$ given by the lifetime difference between the smallest and largest SN progenitor. Considered the uncertainty about the minimum mass of such progenitors, and the details in stellar evolution which weight on the value of $\rm M_{mass}$, we adopt $t_{\rm SN} \sim 25$ Myr as a reasonable compromise.

In general for massive objects like GCs a high explosion rate is expected for the SNe belonging to the FG; as a consequence, most of the SN energy input is thermalized, and a strong wind is driven out of the cluster (e.g. Chevalier & Clegg 1985). We, thus, consider bubbles inflated by a continuous wind rather than by a sequel of instantaneous explosions. On the numerical side, this treatment is supported by the findings of Mac Low & McCray (1988) who showed that discrete explosions can be approximated as continuous events when more than nearly seven SNe explode one after the other. As far as the temporal wind evolution is concerned, Leitherer et al. (2014) showed that SNe belonging to an instantaneous burst release mass and energy at rates only slowly decreasing in time; within our schematiza-

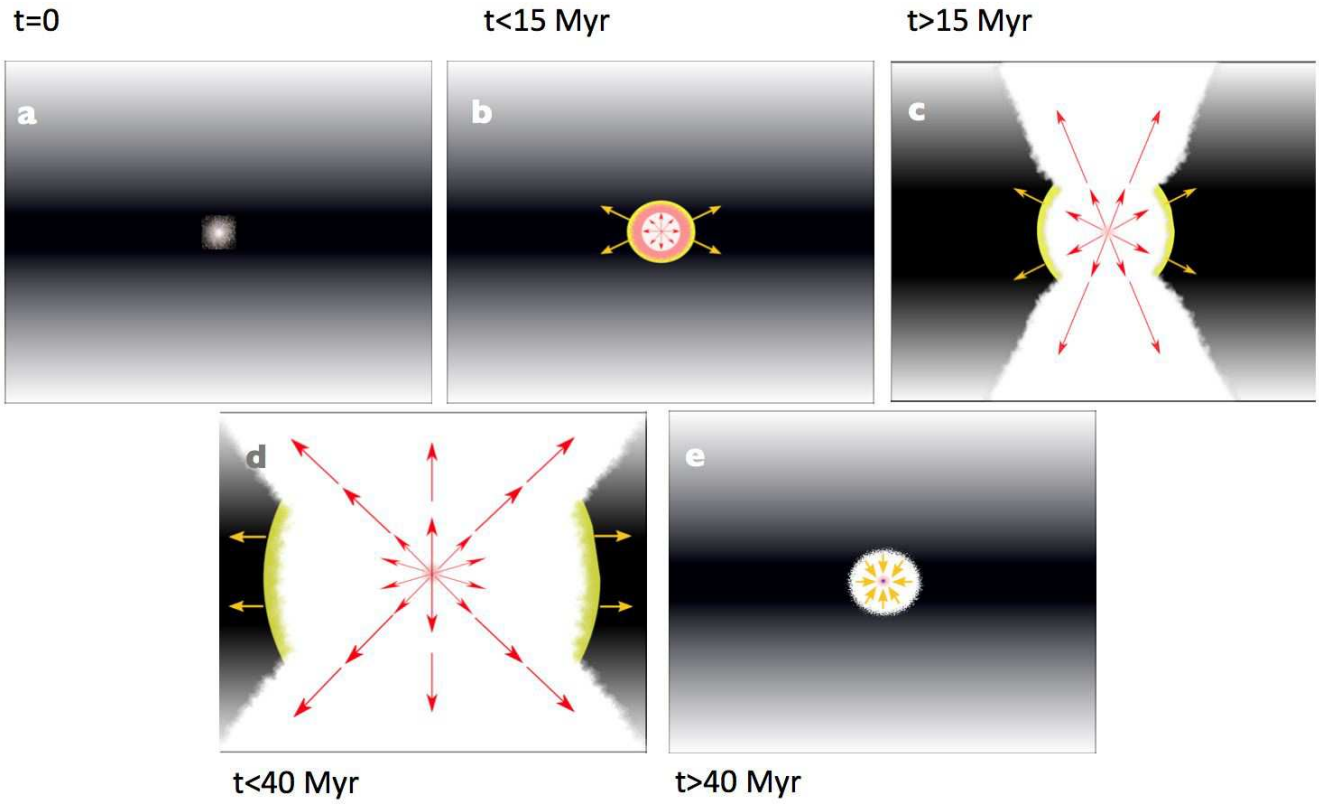

Figure 1. This figure is a very schematic illustration of the evolution throughout the "standard" formation of a two-generation cluster, described by the text equations (we point out that the symmetry in the figure provides just a simplified view; the actual 3D configuration may be more complex because of the turbulence). Times are indicative of the cluster age. Panel *a*: birth of the first stellar generation in the midplane of the stratified medium (grayscale) of a young galactic disk; panel *b*: beginning of the SN II epoch, with expansion of the bubble in the disk. The local gas swept up by the bubble is confined in a cool, dense, thin shell (yellow), while the free expanding wind powered by the SNs (red arrows) is thermalized (red area) after crossing the reverse shock due to the reflection against the contact surface between the ambient gas and the SN ejecta; panel *c*: the bubble expands beyond the disk scale height and the SN wind is lost from the disk; panel *d*: the hole on the disk expand as long the SNs keep exploding. Depending on the parameters, it may still increase in size for a while after the SN activity, until its expansion velocity slows down to the velocity dispersion of the surrounding gas; panel *e*: after the end of the SN II explosions, the disk matter closes up again into the cluster. Depending on the bubble radius, there is time, or not, to form an extreme second generation from the super–AGB ejecta; then star formation includes AGB matter partially diluted with the re-accreted disk gas. Phases described in panels *b* and *e* may also represent the further stop of star formation due to binary delayed SN II explosions (panel *b*) and the successive reaccretion phase, which now includes both the AGB and SN ejecta (panel *e*).

tion we can safely assume these rates to be constant, and we computed them as follows.

The total number of explosions is $N_{\rm SN} = 7 \times 10^{-3}(M_{\rm FG}/{\rm M}_\odot)$, and the total amount of SN ejecta is $M_{\rm SN,ej} = 0.09 M_{\rm FG}$[2]. We thus obtain $\dot{M}_{\rm SN} = M_{\rm SN,ej}/t_{\rm SN}$ and $L_{\rm SN} = N_{\rm SN} E_0/t_{\rm SN}$, respectively, where $E_0 = 10^{51}$ erg is the energy of a single SN. In summary, in our models we assume

$$\dot{M}_{\rm SN} = 3.6 \times 10^{-9} \left(\frac{M_{\rm FG}}{{\rm M}_\odot}\right) {\rm M}_\odot \ {\rm yr}^{-1}, \quad (2)$$

and

$$L_{\rm SN} = 9.0 \times 10^{33} \left(\frac{M_{\rm FG}}{{\rm M}_\odot}\right) {\rm erg \ s}^{-1}. \quad (3)$$

Assuming that all the SN luminosity is transformed in the wind mechanical luminosity [3] $L_{\rm w}$, we obtain a wind terminal velocity $V_{\rm w} = (2L_{\rm w}/\dot{M}_{\rm SN})^{1/2} = 2800$ km s^{-1}.

3 INTERACTION OF THE GC WIND WITH THE SURROUNDING MEDIUM

3.1 Bubble expansion: summary

Before describing the interaction of the GC wind with the surrounding medium, we briefly summarize the evolution of a "standard" spherical bubble, that is, a bubble powered by a constant luminosity wind and expanding through a local uniform gas (Weaver et al. 1977). The wind generated by the sequential supernova explosions produces a hot bubble which expands and sweeps out the ambient medium; this gas is compressed into a shell by a shock located at its leading edge. The kinetic energy of the wind is partly converted into thermal energy by a reverse shock located behind the shell, close to the centre. The shocked ambient medium and the shocked hot wind are separated by a contact discontinuity. In absence of relevant radiative losses, the bubble expands in

[2] Following Iben & Tutukov (1984), we assume that each SN leaves a neutron star of 1.5 M$_\odot$.

[3] Following Calura et al. (cf. 2015) we assume that the residual gas out of which the GC formed is expelled from the cluster by the SN wind.

the energy-conserving regime, and its radius grows in time as $R_{\rm b} \propto t^{3/5}$. Given its high temperature and low density, usually the bubble interior does not cools radiatively; instead, the outer shell, denser and cooler, is radiative, and usually collapses quite soon. However, radiative losses from the shocked ambient medium have little effect on the expansion of the bubble which preserves the same time dependence, just reducing its expansion velocity of about 13% (Weaver et al. 1977). For this reason in the following we still refer to this stage, although somewhat improperly, as to the "energy-conserving regime".

Under certain conditions, it may happen that the radiative cooling of the bubble hot interior is large enough to affect the bubble expansion. In this case, the thermal pressure of the shocked wind is essentially absent, and the reverse shock moves close to the shell. The wind energy in such a radiative bubble is not conserved, but the wind momentum is: the wind pushes directly onto the shell, transferring its momentum. This is the so-called momentum-conserving regime, with $R_{\rm b} \propto t^{1/2}$ (Steigman et al. 1975).

Finally, we warn the reader that, to make computations easier, in the following the time t is computed starting from the beginning of the SN explosions. Therefore, the age $t_{\rm age}$ of of the cluster is $t_{\rm age}+t_0$, where $t_0 \sim 10$ Myr is the lifetime of a star with a mass of 20 $M_\odot$.

We now go back to our model and see how the above concepts come into play.

3.2 First expansion stage: spherical expansion

The bubble preserves a nearly spherical shape as long as it expands within the disk. During the expansion the pressure of the bubble decreases, and two possibilities are in order: *i*) if the pressure decreases down to the interstellar matter (ISM) pressure when the bubble radius is smaller than $H_{\rm eff}$ the bubble stalls. At this point, since the bubble is in a gravitational field, it is likely to be subject to the Rayleigh-Taylor instability; as a consequence, the ambient gas can mix with the bubble interior, leading to the cooling and collapse of the bubble itself; *ii*) if the radius reaches $H_{\rm eff}$ the bubble breaks out. Following Koo & McKee (1992), the characteristic wind luminosity that determines whether a bubble will be able to break out of the disc is

$$L_{\rm br} = 53.7 \rho_0 H_{\rm eff}^2 \sigma_0^3 \ \ {\rm erg\ s^{-1}}, \tag{4}$$

where ρ_0 is the midplane density. For the moment we consider cases for which $L_{\rm w} > L_{\rm br}$, leading to bipolar flows often observed in starburst galaxies (e.g. Strickland & Heckman 2009), and postpone the discussion of the cases in which the opposite is true (see sect. 4.1). This first stage ends at the time at which the breakout occurs [4] (see Appendix A)

$$t_{\rm br,6} = 0.19 H_{\rm eff,2}^{5/3} \left(\frac{L_{41}}{n_0}\right)^{-1/3}, \tag{5}$$

where n_0 is the numerical density of the ambient gas, $t_{\rm br,6} \equiv t_{\rm br}/{\rm Myr}$, $L_{41} \equiv L_{\rm w}/(10^{41}\ {\rm erg\ s^{-1}})$, and $H_{\rm eff,2} \equiv H_{\rm eff}/10^2$ pc.

[4] Following Mac Low & McCray (1988), it can be shown that, given the values of the parameters, usually the bubble is still in the energy-conserving stage when it breaks out.

3.3 Second expansion stage: wind momentum conservation

At the breakout the shell suddenly accelerates. This acceleration causes the disruption of the shell by the Rayleigh-Taylor instability, and the wind blows directly out of the planar medium (e.g. Koo & McKee 1992). As a consequence, the SN ejecta are quickly lost by the galaxy, without any significant pollution of the local ISM; this is a crucial point for the chemical evolution of the cluster, as the different stellar populations within the majority of the GCs do not show appreciable differences in the abundance of iron. At the breakout the bubble pressure drops as the hot interior leaks out. At this stage the wind impinges directly on the inner surface of the portion of the shell which is moving parallel to the plane; this shell, which we assume cylindrical, expands now in a wind momentum-conserving regime.

The shell radius grows to a maximum values, the stalling radius $R_{\rm st}$, where the shell velocity drops to the dispersion velocity σ_0 of the ambient medium; $R_{\rm st}$ is equal to $R_{\rm eq}$, the radius where the wind ram pressure equals the pressure of the ISM. The expansion ceases and the shell, whose density is now similar to that of the local gas, stalls merging into the ISM.

It is possible, however, that the shell does not stalls at the equilibrium radius. This can occur because when the shell switches to the wind momentum-conserving regime at a radius $\sim H_{\rm eff}$, it has a momentum given by the energy-conserving solution that is higher than the momentum expected at that radius in a "pure" momentum-conserving regime (when the expansion is momentum conserving from the beginning). Therefore the shell overruns the equilibrium radius because its velocity is higher than σ_0, and keeps expanding although the wind ram pressure is lower than the ambient pressure. Later, when the shell velocity becomes equal to σ_0, the hole stalls.

It may happen that the shell is still expanding at $t > t_{\rm SN}$, when the wind has already ceased to blow. In this case the hole enters a third dynamical stage.

3.4 Third expansion stage: shell momentum conservation

This third stage starts at $t_{\rm SN}$, when the supernovae cease to explode. Even in absence of the wind the shell continues to expand because of the inertia of the swept-up mass. Eventually, however, it stalls at $R_{\rm st}$.

3.5 Analytical description of the expansion phase

In Appendix A we present a derivation of the the expansion law of the bubble for each of the three dynamical stages:

$$R_{\rm b,2}(t) = \begin{cases} 2.7 \mathcal{L}^{1/5} t_6^{3/5} & \text{if } t \le t_{\rm br} \\ H_{\rm eff,2} \left(\frac{t}{t_{\rm br}}\right)^{\beta} & \text{if } t_{\rm br} < t \le t_{\rm SN} \\ (3\beta \frac{R_{b,2}^3(t_{\rm SN,6})}{t_{\rm SN,6}} (t_6 - t_{\rm SN,6}) + & \\ + R_{b,2}^3(t_{\rm SN,6}))^{1/3} & \text{if } t > t_{\rm SN} \end{cases} \tag{6}$$

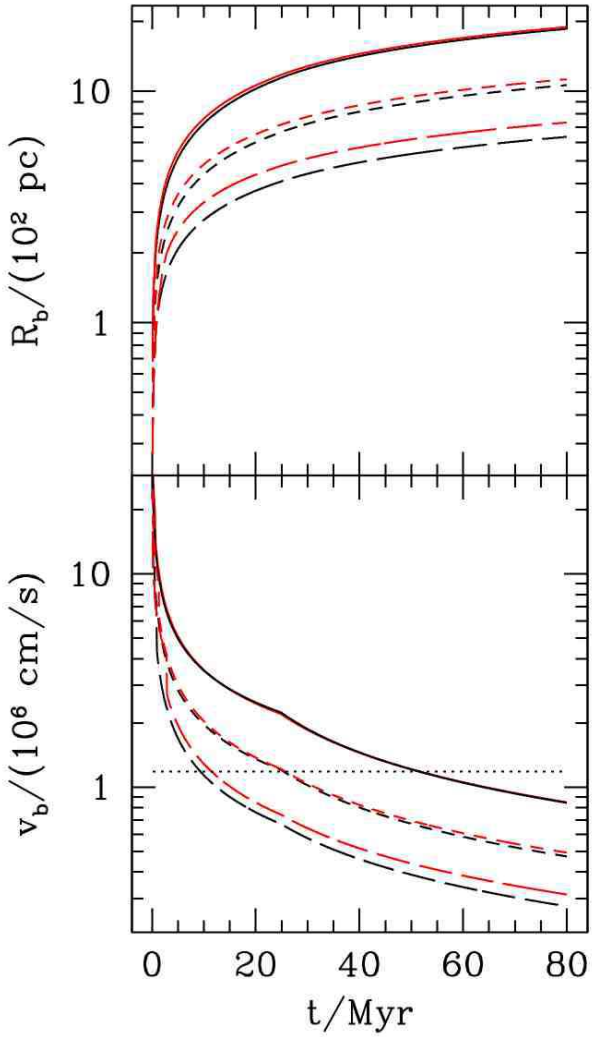

Figure 2. Bubble radii (upper panel) and expansion velocities (lower panel) for different values of the parameters: $\mathcal{L} = 0.01$ (long-dashed lines), $\mathcal{L} = 0.1$ (short-dashed lines), $\mathcal{L} = 1$ (solid lines); black lines are for $H_{\rm eff,2} = 1$, and red lines for $H_{\rm eff,2} = 2$. The horizontal dotted line in the lower panel indicates the velocity dispersion of the ambient medium.

Here lenghts are in 0.1 kpc and times in Myr. The dependence of the bubble expansion on L_{41} and n_0 occurs only through the ratio $\mathcal{L} \equiv L_{41}/n_0$, which is the main parameter regulating the bubble evolution; this evolution depends also on a second parameter, $H_{\rm eff}$, which however plays a secondary role, as shown in Figure 2. Finally, β has a weak dependence on $\mathcal{L}$ and $H_{\rm eff}$, as described in the Appendix A.

As an example, we show in the lower panel of Fig. 2 a horizontal dotted line corresponding to a dispersion velocity $\sigma_0 = 1.15 \times 10^6$ cm s^{-1} (equivalent to the isothermal sound speed of the ambient medium whose temperature is assumed to be 10^4 K). The intersection of this line with the curves describing the expansion velocity of different models determines the time $t_{\rm st}$ at which such models reach the radius $R_{\rm st}$ and stop their growth.

3.6 Bubble contraction

As pointed out in sect. 3.3, when the bubble reaches the radius $R_{\rm st}$ it loses its particular structure, and can be simply regarded as a hole in the disk rather than a bubble; however, in order to avoid confusion with symbols and nomenclature we continue to refer to such hole as "bubble". At $R_{\rm st}$ the wind ram pressure is inadequate to hold the bubble at this radius, and the ambient gas encroaches into the cavity with velocity σ_0 (Heiles 1987; D'Ercole 1992; Koo & McKee 1992); in the following we will refer to this stage of progressive replenishment and reduction of the hole as "bubble contraction" or "bubble shrinking".

If the GC wind is still active (that is, if $t < t_{\rm SN}$), a steady state configuration is established at the equilibrium radius where the ram pressure of the wind balances the ambient pressure, $\rho_{\rm w}(R_{\rm eq})V_{\rm w}^2 = P_0$:

$$R_{\rm eq,2} = 41.43 \left(\frac{\mathcal{L}}{V_{\rm w,8}\sigma_{0,6}^2} \right)^{1/2}, \qquad (7)$$

where $V_{\rm w,8} \equiv V_{\rm w}/10^8$ cm s^{-1}, and $\sigma_{0,6} \equiv \sigma_0/10^6$ cm s^{-1}. Once the GC wind ceases, at $t \geq t_{\rm SN}$, the bubble shrinks again completing its contraction at the time

$$t_{\rm co} = t_{\rm SN} + R_{\rm eq}/\sigma_0. \qquad (8)$$

For higher values of $\mathcal{L}$, the receding bubble reaches $R_{\rm eq}$ at $t > t_{\rm SN}$, and therefore contracts directly toward the centre after

$$t_{\rm co} = t_{\rm st} + R_{\rm st}/\sigma_0. \qquad (9)$$

The dynamical behaviour of the bubbles is summarized in Fig. 3. As an example, we report in the upper panel just the case with $\sigma_{0,6} = 1.17$ and $H_{\rm eff,2} = 1$; the general behaviour of other cases is similar, but we do not show them in order to avoid to clutter the figure. The solid line indicates the maximum radius reached by bubbles with different $\mathcal{L}$, while the dashed line shows the equilibrium radius at which bubbles with $\mathcal{L} \leq 0.1$ settles during the successive contraction, "waiting" for the end of the SN activity; after $t_{\rm SN}$ the contraction is restored until its conclusion. This expansion and the successive "two–step" contraction are represented by the three arrows in the low $\mathcal{L}$ region of the diagram. The two arrows on the right side show that bubbles with $\mathcal{L} > 0.1$ contract totally and directly after reaching their maximum extension. For these bubbles the dashed line indicating the equilibrium radius is meaningless; we show only the portion of this line for $\mathcal{L} \leq 0.1$ to point out that only this segment is meaningful. The critical value $\mathcal{L} = 0.1$ separating the behaviour of the collapsing bubbles varies for different values of the parameters σ_0 and $H_{\rm eff}$, but the overall bubble dynamics remains qualitatively unchanged.

The lower panel of Fig. 3 shows the lifetime of bubbles with different $\mathcal{L}$. It has been computed by equation (8) or equation (9), depending on the value of $\mathcal{L}$.

4 DISCUSSION

Figure 3, together with the results of previous simple chemical evolution models based on the AGB scenario (D'Ercole et al. 2010, 2012), constrain the ambient medium properties needed to have a viable dilution mechanism. As

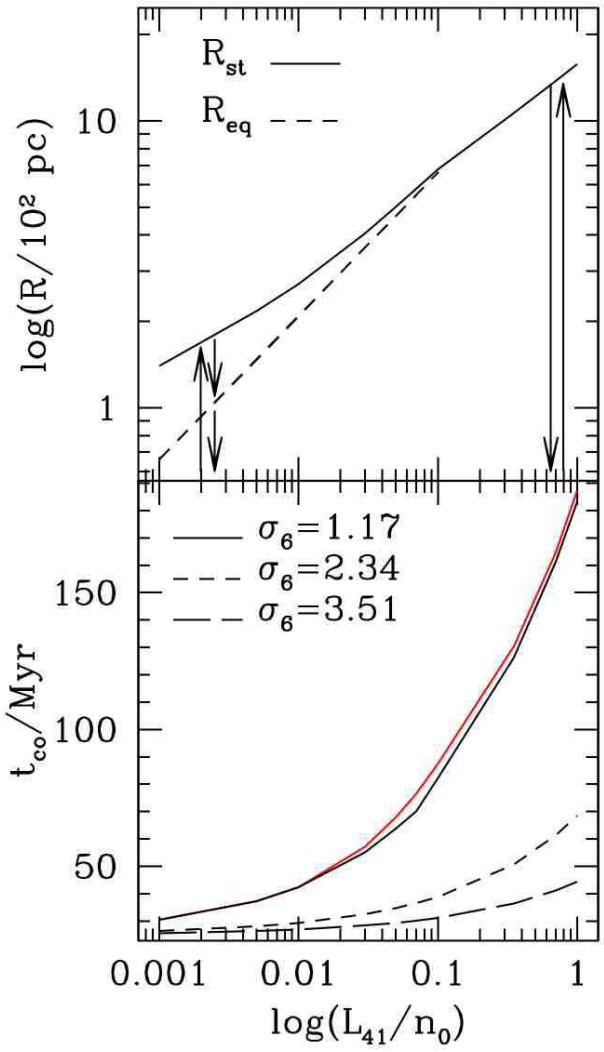

Figure 3. Upper panel: stalling radius $R_{\rm st}$ (solid line) and equilibrium radius $R_{\rm eq}$ (dashed line) as function of $\mathcal{L}$ for $H_{\rm eff,2} = 1$. The behaviour of these radii for $H_{\rm eff,2} = 2$ is similar, but we do not show them to avoid to clutter the figure. For the same reason we show only the case $\sigma_6 = 1.17$. The arrows on the left side indicate schematically the behaviour of the radius of bubbles with $\mathcal{L} \leq 0.1$: it grows up to $R_{\rm st}$ and then shrinks reaching $R_{\rm eq}$ at a time $t < t_{\rm SN}$. Here the bubble settles until $t_{\rm SN}$; later on it contracts definitively. The evolution of bubbles with $\mathcal{L} > 0.1$ is schematized by the two arrows on the right side: in this case the bubble, after reaching its maximum size, contracts directly until it closes. For these bubbles, the portion of the dashed line extending beyond $\mathcal{L} = 0.1$ is meaningless and is not shown in the figure (see text). Lower panel: lifetime of a bubble as function of $\mathcal{L}$ for three values of σ_0. For the case $\sigma_0 = 11.7$ km s^{-1} we show the case $H_{\rm eff} = 100$ pc (black line) and $H_{\rm eff} = 200$ pc (red line).

shown in (D'Ercole et al. 2010, 2012), in order to form a suitable amount of E stars – for example, 18% of the present GC mass as in NGC 2808 (Carretta et al. 2009a) – pure undiluted AGB ejecta must flow in the cluster centre for about 20 Myr after the end of the SN II activity. After this time a substantial episode of dilution is needed to form the Intermediate population; in NGC 2808 it represents about 32% of the total, and nearly 40–50 % of its mass is composed by accreted pristine gas.

The above requisites indicate that the bubble must have a lifetime of about 45 – 50 Myr; from Fig. 3 we see that, for the model with $\sigma_{0,6} = 1.17$, it must be $0.01 \lesssim \mathcal{L} \lesssim 0.02$, and that the maximum extension reached by the bubble for $H_{\rm eff,2} = 1$ ($H_{\rm eff,2} = 2$) is $R_{\rm st} \sim 300$ pc ($R_{\rm st} \sim 400$ pc). Assuming $M_{\rm FG} = 10^7$ M$_\odot$, it turns out that $\rho_0 \sim 1.5 - 2.0$ M$_\odot$ pc^{-3}, $\Sigma \sim 300 - 800$ M$_\odot$ pc^{-2}, and $P_{0,6} \sim 1$, where $P_{0.6} \equiv P_0/(10^6\,\kappa$ cm^{-3} K), and κ is the Boltzmann constant.

The above figures are order of magnitudes larger than those of the Milky Way. Yet, they are at the low end of gas-rich, normal galaxies at $z > 2$ which may reach pressures $P/\kappa \gtrsim 10^8$ K cm^{-3}, $\sigma_0 = 10 - 100$ km s^{-1} (but see sect. 4.1), and surface densities $\Sigma > 10^3$ M$_\odot$ pc^{-2} (cf. Kruijssen 2015, and references therein).

Our result shows that our model requires properties of the ambient surrounding GCs during their formation and early evolution consistent with those of "normal", star-forming disk galaxies observed at redshift $z > 2$, a conclusion in agreement with the findings of Kruijssen (2015).

We have discussed in detail the model with $\sigma_{0,6} = 1.17$ illustrated in the lower panel of Figure 3. In the same panel we also show the, possibly more realistic, cases with $\sigma_{0,6} = 2.34$ and $\sigma_{0,6} = 3.51$. Increasing σ_0 leads to values of $\mathcal{L}$ appropriate for a NGC 2808-like GC which span a broader range and are shifted to higher values.

Models with low values of $\mathcal{L}$ are suitable to describe GCs where the dilution is expected to occur quite soon (i.e. clusters in which the Extreme population is absent, as M4 (NGC 6121) (D'Ercole et al. 2010). The sequence of events for these clusters would be identical to those exhibiting an extended Na–O anticorrelation (cf. Fig. 1) with the only difference being the smaller size reached by the bubble.

Models with large values of $\mathcal{L}$ require a long time to shrink (see Fig. 3). If this time is longer than the time after which delayed SNe II or Type Ia supernovae (SNe Ia) start to explode (see sect. 4.2), the bubble does not contract completely and the cluster does not accrete pristine gas. In this case the GC should host a SG population composed only by extreme stars formed out of the undiluted AGB ejecta during the time interval between the end of the single SNe II activity and the beginning of the late SN II and/or SN Ia explosions. D'Antona et al. (2016) hypothesize that this could be the case of the globular cluster NGC 2419 for which the results of Di Criscienzo et al. (2015) and Cohen et al. (2011) suggest that the second generation is entirely or mostly Extreme.

More in general, being the bubble lifetime an inceasing function of $\mathcal{L}$, and thus of the initial cluster mass, a correlation occurs between the strength of the signature of the AGB chemical pollution and the cluster mass. This correlation may be weak, as we have seen that this lifetime depends also on several other physical inputs, but nevertheless it should be present. A particular case concerns the helium content of the second generation stars. We noticed above that the presence of a high helium (Y∼0.35-0.38) population in the most massive clusters is the outcome of stars from undiluted AGB ejecta. In addition, as a consequence of the model presented here we expect a correlation between the *average* helium content of the second generation and the cluster mass. In fact, clusters with smaller masses are characterized by smaller AGB ejecta rate and shorter reaccretion

time, and fewer or no stars may form from gas in which the ejecta are not strongly diluted.

Other evolutionary paths for the bubble are also possible. In fact, from equation (4) we know that, if $\mathcal{L} \lesssim \mathcal{L}_{\rm br} \equiv 5 \times 10^{-5} H^2_{\rm eff,2} \sigma^3_{0,6}$, the bubble is not able to break-out and its evolution is rather different from that described in section 2; is this a realistic option? In the following, we discuss two main cases.

4.1 The SN II main phase

Given its strong dependence on σ_0, high values of $\mathcal{L}_{\rm br}$ are attained for large values of the velocity dispersion which may be as high as $\sigma_{0,6} = 10$ in star forming galaxies at $z = 2$. This value, however, is rather extreme; Wisnioski et al. (2015) shows that the mean velocity dispersion is around $\sigma_{0,6} = 5$, and a similar result is obtained by Tacconi et al. (2013). Moreover, a possible lack of an adequate resolution may lead to overestimated values of the velocity dispersion (Newman et al. 2013).

However, despite the above arguments, and although GCs usually form in "normal" galaxies, it cannot be excluded that in some clusters the wind is not strong enough to satisfy the conditions required for a break-out. In this case the bubble, which remains approximately spherical, expands up to the stalling radius, and keeps such size until $t_{\rm SN}$, after that contracts in a time $\sim R_{\rm st}/\sigma_0$. The SN II ejecta are all contained within the bubble, but they will not necessarily contaminate the gas out of which the SG will form.

In fact, it is possible that the cluster is not exactly at rest with respect to its ambient gas; even a low relative velocity is enough to allow the cluster to move away from the centre of the bubble which instead remains in its original position. It is also possible that the cluster reaches the shell; the bubble then becomes distorted and its leading edge acquires the shape of a bow-shock (Weaver et al. 1977; Brighenti & D'Ercole 1994). In any case, at the end of the SN II activity, the bubble contracts toward the centre, driving there its content of SN ejecta; being the GC off-centre, the SN ejecta are not involved in the SG star formation occurring in the cluster core (see also sect. 5.4).

4.2 The delayed binary SN II phase

It is well known that SN II may occur also after the end of the main phase due to the evolution of single stars. In fact, in interacting binaries having mass components below the minimum mass for explosion, mass transfer may push the accreting component beyond such minimum (van Kerkwijk & Kulkarni 1999; Portegies Zwart & Yungelson 1999; Tauris & Sennels 2000). The frequency of such events may vary strongly from a cluster to another [5]. We do not consider the case in which $\mathcal{L}_{\rm delSN\ II} \gtrsim \mathcal{L}_{\rm br}$, as it is evident that this would fully preclude re-accretion, and also hamper the formation of second generation stars for a long hiatus. We are here more interested in the cases $\mathcal{L}_{\rm delSN\ II} \lesssim \mathcal{L}_{\rm br}$. We can distinguish different possibilities:

1) Delayed SN II explosions isolated in time: as already discussed in D'Ercole et al. (2008) one isolated SN explosion will not produce significant dynamical effects: the small bubble will close soon enough and the supernova ejecta will take part in the cooling flow and contribute to the formation of new stars in the core. Anyway, one such SN II explosion will only disperse into the medium ~ 0.07 M$_\odot$ of iron and a more relevant 0.5 M$_\odot$ of oxygen. Whether or not this material may cause a visible spread in the abundances of second generation stars depends on the amount of polluted material and on the initial cluster metallicity (the lower the metal abundances, the larger will be the effect of oxygen pollution).

2) A phase of delayed SN II explosions extended in time, lasting for several 10^7yr: this case study may lead to the formation of 's-Fe-anomalous clusters'. While most GCs can be considered mono-metallic, with an upper limit to the scatter of iron less than 0.05 dex (Carretta et al. 2009b), in recent years it has been found that there is a small number of objects characterized by an intrinsic internal [Fe/H] abundance dispersions (see Da Costa 2015, for a summary review). The fraction of stars with increased iron content may vary from a few percent to 15–30% (Marino et al. 2015), and the most intriguing characteristic is that the stars with larger [Fe/H] abundances also have higher [s-element/Fe] abundance ratios, requiring an additional s–process element contribution, most probably from AGB–stars, over and above the contribution needed to maintain the abundance ratio as the iron abundance increases (Da Costa 2015). These clusters have been dubbed 's-Fe-anomalous' by Marino et al. (2015). *Both iron groups of 's-Fe-anomalous clusters' show independent O–Na anti correlation.* We discuss in D'Antona et al. (2016) how these groups may be formed from a chemical point of view. Here we show that our model provides a dynamical scenario able to produce the observed chemical properties.

Let us assume that the cluster had time to form a 'first' second generation, after reaccretion of the disk gas (this is necessary to produce the O–Na anticorrelation shown by the low metallicity stars), and that, afterwards, at about 60–70Myr of age, the delayed SN II epoch halts the second–generation star formation for a time $t_{\rm delSN}$. The energy of each supernova will be, as for single supernovae explosions, $E_0 = 10^{51}$ erg and we can assume that the whole luminosity goes into the wind mechanical luminosity. We get $L_{\rm w(del.SN)} = N_{\rm delSN} E_0 / t_{\rm delSN}$. The AGB ejecta become s-process rich when their envelopes experience the effects of numerous episodes of third dredge up, at ∼90–100 Myr of age. Thus we have a typical timescale of $t_{\rm delSN}$=20–40 Myr. For a total number of 10-40 explosions, we obtain $L_{\rm w,delSN} \simeq 0.8 - 6 \times 10^{37}$erg s^{-1}. This value is small enough that indeed $\mathcal{L} < \mathcal{L}_{\rm br}$, and the wind will not freely escape from the disk. The bubble radius may even be so small that it will not reach the cluster periphery (D'Ercole et al. 2008), but this will be sufficient to prevent star formation, until the bubble recollapses into the core. The matter forming this second phase of second generation formation will be enriched both by the ejecta of the supernovae and from the AGB winds, which will now be s–enriched and CNO enriched.

[5] Computing the frequency of delayed SNe II and the extent of the time interval during which they explode requires specific stellar population synthesis models taking into account the fraction of primordial binary systems and their initial properties (e.g. period and mass ratio distribution). More details on the role of the delayed SNe II within the AGB scenario can be found in D'Antona et al. (2016).

We can summarize the time sequence of the events leading to the formation of s-Fe-anomalous clusters as follows:

(i) Formation of SG stars with the iron content equal to that of the FG population: this follows the steps outlined in the paper and schematically illustrated in Figure 1.
(ii) Delayed SN II epoch: a bubble forms (panel b of Fig. 1) and remains confined into the disk, and possibly within the cluster periphery. The iron and oxygen of these supernovae remain confined and mix with the disk gas at the bubble periphery as a result of a number of possible processes, such that Rayleigh-Taylor instability (see sect. 3.2), turbulent mixing layers (Slavin et al. 1993), thermal evaporation (Weaver et al. 1977) and photoevaporation(McKee et al. 1984). The average metallicity of the gas surrounding the bubble increases to $[\mathrm{Fe/H}]_0 + \Delta[\mathrm{Fe/H}]$. Also the AGB winds coming from inside the bubble are locked with the disk gas. Star formation is off for 20–40Myr.
(iii) Recollapse of the bubble and second phase of second generation formation. A burst of star formation occurs from the gas polluted by the delayed SN II and mixed with AGB winds. If the mixing is inhomogeneous, we may still obtain an O–Na anti correlation in stars having iron content $[\mathrm{Fe/H}]_0 + \Delta[\mathrm{Fe/H}]$.
(iv) The timing of this event is such that it occurs close to the beginning of the SN Ia explosions in the cluster, which ends the second star formation epoch.

5 SOME MORE COMPLEXITIES

It is important, in our model, that the disk gas surrounding the cluster remains uncontaminated despite the metals ejected by the SNe; in this way it can give rise, once moved within the cluster, to a SG population with the same iron abundance of the FG one, as observed in most of the clusters (Piotto et al. 2015). In this section we consider some aspects of the model which have been neglected until now, and which could lead to an increment of [Fe/H] of the disk gas. We show that this gas effectively preserves its original chemical composition, at least during the time intervals of interest for the model.

5.1 Asymmetric models

Until now we considered symmetric models where the cluster is located on the galactic midplane. Of course, the cluster may also form off-plane, at a distance $0 \leq h \lesssim H$ from the middle of the disk. In this case the associated asymmetric bubble would preferentially break out of one side of the disk, but not necessarily out of the other; a non negligible fraction of the SN ejecta would then remain trapped within the ISM that, after accretion, would lead to a SG enriched in Fe, at odd with the majority of the observed galactic clusters. Of course, a critical height h_c exists, above which the bubble is effectively unable to cross entirely the disk thickness. This critical height depends, of course, on L_w, n_0 and H, but finding out such dependence requires hydrodynamic simulations which are beyond the scope of this paper. However, we can get some insight into the behaviour of an asymmetric bubble from the numerical models of Mac Low & McCray (1988). These authors considered a plane parallel exponential atmosphere with $H_{\mathrm{eff},2} = 1$ and $n_0 = 1$ cm^{-3} crossed by a bubble with $\mathcal{L} = 10^{-3}$; they find $h_\mathrm{c} = 0.6 H_\mathrm{eff}$, while for $h < h_\mathrm{c}$ the bubble blows out of the opposite side at $t < 1.2$ Myr. Being $\mathcal{L} \sim 0.01$ in our models, we believe that the bubble easily erupts from the distant side of the plane; scaling the Mac Low & McCray results, this would occur after about 0.6 Myr.

We also stress that a GC initially placed above the galactic plane is expected to oscillate up and down across the disk with a period (e.g. Shaviv 2006)

$$P_0 \simeq \left(\frac{\pi}{G\rho_0}\right)^{0.5} = 26.42 \left(\frac{\rho_0}{M_\odot\ \mathrm{pc}^{-3}}\right)^{-0.5} \quad \mathrm{Myr}. \tag{10}$$

Thus, for a typical value $\rho_0 = 1$ M$_\odot$ pc^{-3} the cluster crosses the plane two times during the SN activity. These oscillations represent a further degree of flexibility of the model which helps to account for differences among the clusters.

5.2 Potential pollution by the GC wind

In our model we assumed that the ISM on the disk surrounding the cluster is not enriched by the SN metals. We now discuss this assumption. Numerical simulations (e.g. Schiano 1985; Tenorio-Tagle & Muñoz-Tuñón 1997, 1998) show that the wind hitting the shell on the disk is deflected away from the plane, ablating the superficial gas layers of the inner side of the shell and dragging them away. Mac Low & Ferrara (1999) proved that the fraction of SN metals retained by the ISM decreases with the increasing wind power, and is substantially absent for $L_{41} > 10^{-3}$.

In any case, the possible mixing achieved in numerical simulations represents an upper limit because it depends on the numerical diffusion which is usually much greater than the physical one (e.g. Marcolini et al. 2004). The physical diffusion is a rather slow process in warm and cold gas, and this led Tenorio-Tagle (1996) to put forward a scenario for the ISM enrichment in which the metal-enriched blown-out gas remains in the hot rarefied gaseous halo where mixes efficiently. This hot gas than cools, condenses and falls back onto most of the disk evenly after about 10^8 yr. Contrary to other proposed mechanisms such as galactic fountains, turbulence and accretion (cf. Tolstoy et al. 2009; Melioli et al. 2015, and references therein) this framework can explain the absence of significant metal abundance gradients throughout the dwarf galaxies, and represents our main current understanding of the ISM pollution.

We thus conclude that the strong winds considered in our model do not significantly contaminate the disk, in particular for the interval of time of interest, which is shorter than 10^8 yr.

5.3 Triggered star formation

The expanding shell may trigger star formation (SF) by gravitational collapse of swept-up gas as well as by compression of pre-existing gas clouds (e.g. Elmegreen 2011). The SNs belonging to this triggered stellar population could contaminate the surrounding disk gas with their iron; then this gas, once moved into the cluster at the end of the GC wind, would contribute to the formation of a stellar SG with

a [Fe/H] higher than that of the FG. Actually, this could occur if all the iron released by SNs were "immediately" available for ambient gas pollution; this is not the case, however. Stars formed within clouds engulfed and overrun by the expanding shell, as well as stars formed within the dense shell, are exposed to the GC wind, and the ejecta of the SNs belonging to this stellar population are quickly vented away. Bubbles powered by clusters with $\mathcal{L} \lesssim 0.1$ (see Fig. 3) stall (interrupting any star formation) when the GC wind is still blowing, and no ISM pollution is expected. For $\mathcal{L} \gtrsim 0.1$ the shell keeps expanding for a while after the SN stage; in this phase, however, the shell is only weakly supersonic, and its effectiveness in triggering SF is most likely reduced (Elmegreen 2011). Moreover, part of the iron released by SNs formed in this period should be presumably lost above the disk, at least for a while (see sect. 5.2). Finally, only a few clusters are expected to have $\mathcal{L} > 0.1$; we can speculate that pollution from these supernovae may have played a role in those clusters where large iron spreads are found, such as ω-Cen, M54 and possibly NGC 6273 (Yong et al. 2016, and references therein).

5.4 GC motion

So far we considered a cluster at rest along the disk relative to the surrounding gas. This is a quite reasonable assumption; in fact, dwarf galaxies rotate as solid bodies, allowing the GC to remain very near its birth place on time-scales of $\sim 10^8$ yr (Warren et al. 2011, and references therein), shorter than those of interest in our model. In any case, we discuss here some general aspects of the influence of the GC motion. Being the GC wind supersonic, a bow shock forms head of the cluster; the stagnation point, that is the point where the ram pressure of the wind balances the ISM pressure is located at the stand-off distance (e.g. Draine 2011)

$$l_{\rm off,2} = 41.43 \left(\frac{\mathcal{L}}{V_{\rm w,8} \left(\sigma_{0,6}^2 + v_{\rm GC,6}^2 \right)} \right)^{1/2}, \qquad (11)$$

where $l_{\rm off,2}$ is the stand-off distance in unit of 100 pc, and $v_{\rm GC,6}$ is the GC velocity relative to tha ambient gas in unit 10^6 cm s^{-1} (note that the above equation is a generalization of equation (7) taking into account the ISM ram pressure). Once the wind stops blowing, the surrounding gas reaches the GC in a time $l_{\rm off}/(v_{\rm GC} + \sigma_0)$, and successively overruns it. As the ISM flows through the cluster, part of it can be accreted provided that $\sigma_*^2 \gtrsim \sigma_0^2 + v_{\rm GC}^2$, where σ_* is the central stellar velocity dispersion of the cluster (e.g. Naiman et al. 2011). We conclude that the delayed accretion may occur earlier, but is not hampered by the motion of the cluster.

To give an even approximate estimate of the mass accreted by the cluster is not an easy task. While for a point mass accretor the mass accretion rate can be assessed by the Bondi-Hoyle-Lyttleton formula (Bondi 1952), an analogous simple analytical formula for the accretion onto core potentials does not exist, and one must resort to hydrodynamic simulations. Naiman et al. (2011) performed a number of 2D numerical simulations appropriate for different astrophysical contexts. They find that, in general, the accumulation of external gas occurs during an initial period lasting 10-100 sound crossing times $t_{\rm cr}$ of the cluster; eventually a steady configuration is established, and the gas accumulated into the cluster ceases to grow appreciably [6].

The parameters of model A of Naiman et al. (2011) resemble those met in our paper ($v_{\rm GC} = 2\sigma_0 = 2 \times 10^6$ cm s^{-1}, $n_0 = 100$ cm^{-3}) although $M_{\rm GC} = 3.5 \times 10^5$ M$_\odot$ is lower than the cluster masses considered in the present article. It turns out that the accreted mass is $M_{\rm acc} = 0.05 M_{\rm GC}$, and that this accretion occurs in a time $\sim 10 - 100\ t_{\rm cr} \sim 1 - 10$ Myr. Following Naiman et al. (2011), the gas accumulated into the core may reach densities as high as $10^4 \rho_0$; the local free-fall time is then ~ 0.035 Myr, and stars are expected to form rather quickly.

Although this is a very promising result as it suggests that the cluster can indeed re-accrete the correct amount of needed pristine gas (see, e.g., D'Ercole et al. 2010, 2011, 2012), we strongly emphasize that additional simulations are necessary which include the gas shed by the AGB stars as well as the formation of SG stars, two ingredients which are absent in the Naiman et al. (2011) models[7].

5.5 Multiple GCs

The model presented in the previous sections refers to the evolution of a single bubble. Although the formation of isolated GCs cannot be excluded (Bekki 2012), the formation of numerous clusters can effectively occur. We have seen that the typical time-scale for the evolution of a single bubble is $\tau \lesssim 10^8$ yr; after this time the ISM essentially recovers its initial distribution on the disk. Therefore, if a second cluster forms after a time longer than τ, the two bubbles evolve individually. If, instead, more clusters form at the same time, the single bubbles coalesce forming a superbubble which eventually contracts at the end of the SN stage. As the superbubble shrinks, the clusters wthin the hole are overrun by the flowing ISM, accreting some of it as discussed in sect. 5.4. Also in this case a delayed accretion occurs.

6 CONCLUSION

We proposed a scheme for the interaction of the GC wind powered by the SNe II with the surrounding ambient medium. This interaction provides a viable mechanism to supply pristine gas and dilutes AGB ejecta during the SG star formation phase in early Globular Clusters.

We have shown that our proposed mechanism naturally fulfills all the requirements necessary to produce the observed Na-O anticorrelation in the context of the AGB model. Initially, the spherical SN wind drives the expansion of a bubble that, in most cases, breaks out of the gaseous disk where the GC is located. As a consequence, almost all of the SN ejecta is lost along the vertical direction, while the

[6] The isothermal models of Naiman et al. (2011) are obtained assuming a specific heats ratio $\gamma = 1.01$. If a full treatment of the radiative cooling were considered, then a steady state may not exist (Naiman, private communication).

[7] Simulations taking into account sources and sinks of gas can be found in literature, but they are intended to study the accretion of intracluster medium onto galaxies in clusters (e.g. Balsara et al. 1994, and references therein), thus exploring a region of the parameter space of no interest here.

portion of the wind moving mainly parallel to the midplane continues to drive the growth of a hole through the gaseous disk. Some time after the SN activity, the hole starts to contract carrying the surrounding ambient gas, *with pristine abundances*, toward the cluster. The contraction takes a certain period of time during which the ejecta of the massive AGB stars collect within the GC centre and Extreme, O-poor, He-rich stars can form. Once the ambient medium reaches the cluster, it mixes with the AGB ejecta, and Intermediate stars form out of this mixture.

The results of the mechanism presented here are consistent with some still unexplained observational results. In particular, in agreement with observations, only clusters with large $\mathcal{L} = L_{\rm w}/n_0$, and thus mainly clusters with large initial masses, can form an extended Na-O anticorrelation, while the lower values of $\mathcal{L}$ expected for clusters with lower masses do not allow the formation of O-poor, He-rich Extreme stars. In general, a correlation between the spread in helium and the cluster mass is an outcome of the proposed model. Moreover, the pristine gas involved in the dilution is not enriched in iron, giving rise to a SG with the same [Fe/H] of the FG stars, as often found in the observed GCs.

We finally conjectured that the presented scenario may also explain the s-Fe-anomalous clusters where the stars are divided into two main groups with different iron abundances, each group exhibiting an independent O–Na anticorrelation, and with the iron–richer group showing an enhancement of s–process elements. In fact, assuming that few tens of delayed SN II start to explode a short while after the end of the single SNe II explosions, and supposing that such activity lasts for 20–40 Myr, a second bubble forms which, however, stalls before breaking out. The SN ejecta remain trapped into the bubble, and fall back into the cluster when the bubble contracts. This leads to the formation of Intermediate stars in the same way as the collapse of the first bubble did; but the matter forming this second burst of SG stars is enriched with the SN ejecta, giving rise to a bimodality in the iron distribution of the stellar populations.

ACKNOWLEDGEMENTS

We thank the anonymous referee for her/his useful comments. Fruitful discussions with F. Fraternali, J.P. Naiman, R. Sancisi, M. Tosi and G. Zamorani are also acknowledged. F. D'A. and A. D'E. acknowledge support from PRIN INAF 2014 (principal investigator S. Cassisi). E.V. acknowledges support from grant NASA-NNX13AF45G.

REFERENCES

Balsara D., Livio M., O'Dea C. P., 1994, ApJ, 437, 83
Bastian N., Lamers H. J. G. L. M., de Mink S. E., Longmore S. N., Goodwin S. P., Gieles M., 2013, MNRAS, 436, 2398
Bekki K., 2012, MNRAS, 421, L44
Bondi H., 1952, MNRAS, 112, 195
Brighenti F., D'Ercole A., 1994, MNRAS, 270, 65
Calura F., Few C. G., Romano D., D'Ercole A., 2015, ApJ, 814, L14
Carretta E., et al., 2009a, A&A, 505, 117
Carretta E., Bragaglia A., Gratton R., D'Orazi V., Lucatello S., 2009b, A&A, 508, 695
Carretta E., Bragaglia A., Gratton R. G., Recio-Blanco A., Lucatello S., D'Orazi V., Cassisi S., 2010, A&A, 516, A55
Chevalier R. A., Clegg A. W., 1985, Nature, 317, 44
Cohen J. G., Huang W., Kirby E. N., 2011, ApJ, 740, 60
D'Antona F., Vesperini E., D'Ercole A., Ventura P., Milone A. P., Marino A. F., Tailo M., 2016, MNRAS, 458, 2122
D'Ercole A., 1992, MNRAS, 255, 572
D'Ercole A., Vesperini E., D'Antona F., McMillan S. L. W., Recchi S., 2008, MNRAS, 391, 825
D'Ercole A., D'Antona F., Ventura P., Vesperini E., McMillan S. L. W., 2010, MNRAS, 407, 854
D'Ercole A., D'Antona F., Vesperini E., 2011, MNRAS, 415, 1304
D'Ercole A., D'Antona F., Carini R., Vesperini E., Ventura P., 2012, MNRAS, 423, 1521
Da Costa G. S., 2015, ArXiv e-prints (arXiv:1510.00873),
Di Criscienzo M., Tailo M., Milone A. P., D'Antona F., Ventura P., Dotter A., Brocato E., 2015, MNRAS, 446, 1469
Draine B. T., 2011, Physics of the Interstellar and Intergalactic Medium
Elmegreen B. G., 2011, in Charbonnel C., Montmerle T., eds, EAS Publications Series Vol. 51, EAS Publications Series. pp 45–58 (arXiv:1101.3112), doi:10.1051/eas/1151004
Heiles C., 1987, ApJ, 315, 555
Iben Jr. I., Tutukov A. V., 1984, ApJ, 284, 719
Koo B.-C., McKee C. F., 1992, ApJ, 388, 93
Koyama H., Ostriker E. C., 2009, ApJ, 693, 1346
Krause M., Charbonnel C., Decressin T., Meynet G., Prantzos N., 2013, A&A, 552, A121
Kravtsov A. V., Gnedin O. Y., 2005, ApJ, 623, 650
Kroupa P., 2001, MNRAS, 322, 231
Kruijssen J. M. D., 2015, MNRAS, 454, 1658
Leitherer C., Ekström S., Meynet G., Schaerer D., Agienko K. B., Levesque E. M., 2014, ApJS, 212, 14
Lequeux J., 2005, The Interstellar Medium, doi:10.1007/b137959.
Mac Low M.-M., Ferrara A., 1999, ApJ, 513, 142
Mac Low M., McCray R., 1988, ApJ, 324, 776
Marcolini A., Brighenti F., D'Ercole A., 2004, MNRAS, 352, 363
Marino A. F., et al., 2015, MNRAS, 450, 815
McKee C. F., van Buren D., Lazareff B., 1984, ApJ, 278, L115
Melioli C., Brighenti F., D'Ercole A., 2015, MNRAS, 446, 299
Naiman J. P., Ramirez-Ruiz E., Lin D. N. C., 2011, ApJ, 735, 25
Newman S. F., et al., 2013, ApJ, 767, 104
Piotto G., et al., 2015, AJ, 149, 91
Portegies Zwart S. F., Yungelson L. R., 1999, MNRAS, 309, 26
Renzini A., et al., 2015, MNRAS, 454, 4197
Schiano A. V. R., 1985, ApJ, 299, 24
Shaviv N. J., 2006, in Frisch P. C., ed., Astrophysics and Space Science Library Vol. 338, Solar Journey: The Significance of our Galactic Environment for the Heliosphere and Earth. p. 99
Slavin J. D., Shull J. M., Begelman M. C., 1993, ApJ, 407, 83
Smartt S. J., 2009, ARA&A, 47, 63
Spitzer L., 1978, Physical processes in the interstellar medium, doi:10.1002/9783527617722.
Steigman G., Strittmatter P. A., Williams R. E., 1975, ApJ, 198, 575
Strickland D. K., Heckman T. M., 2009, ApJ, 697, 2030
Tacconi L. J., et al., 2013, ApJ, 768, 74
Tauris T. M., Sennels T., 2000, A&A, 355, 236
Tenorio-Tagle G., 1996, AJ, 111, 1641
Tenorio-Tagle G., Muñoz-Tuñón C., 1997, ApJ, 478, 134
Tenorio-Tagle G., Muñoz-Tuñón C., 1998, MNRAS, 293, 299
Tolstoy E., Hill V., Tosi M., 2009, ARA&A, 47, 371
Warren S. R., et al., 2011, ApJ, 738, 10
Weaver R., McCray R., Castor J., Shapiro P., Moore R., 1977, ApJ, 218, 377
Wisnioski E., et al., 2015, ApJ, 799, 209

Yong D., Da Costa G. S., Norris J. E., 2016, preprint, (arXiv:1603.08606)
de Mink S. E., Pols O. R., Langer N., Izzard R. G., 2009, A&A, 507, L1
van Kerkwijk M. H., Kulkarni S. R., 1999, ApJ, 516, L25

APPENDIX A: BUBBLE EXPANSION IN A STRATIFIED MEDIUM

Here we consider the interaction of a GC wind with a surrounding stratified medium with an effective scale height $H_{\rm eff}$ and a midplane density ρ_0. The GC wind drives a bubble whose expansion can be divided in three stages.

As long as the bubble radius is shorter than $H_{\rm eff}$, it can be assumed that the bubble is expanding in an uniform medium with density ρ_0, and its radius $R_{\rm b}$ is given by (Weaver et al. 1977)

$$R_{\rm b,2}(t) = 2.7 \left(\frac{L_{41}}{n_0}\right)^{1/5} t_6^{3/5}, \tag{A1}$$

where $R_{\rm b,2} \equiv R_{\rm b}/\,100\,{\rm pc}$, L_{41} is the wind luminosity in units of 10^{41} erg s^{-1}, n_0 is the numerical density of the ambient medium in cm^{-3}, and t_6 is the time in Myr. As the wind is very powerful, the bubble eventually breaks out at the breaking time

$$t_{\rm br,6} = 0.19 H_{\rm eff,2}^{5/3} \left(\frac{L_{41}}{n_0}\right)^{-1/3} \tag{A2}$$

obtained from equation (A1) for $R_{\rm b} = H_{\rm eff}$.

This time marks the end of the first stage and the beginning of the second dynamical phase. At the breakout the shell suddenly accelerates. This acceleration provokes the disruption of the shell by the Rayleigh-Taylor instability, and the wind blows directly out of the planar medium (e.g. Koo & McKee 1992). From this time forth we focus on the "cylindrical hole" in the planar gas which still keeps expanding under the action of the fraction $f(R{\rm b}, H_{\rm eff})$ of the isotropic wind intercepted by its internal wall. After the breakout, the hot internal gas leaks out and the internal pressure of the bubble drops; the wind thus impinges directly on the cylindrical shell which thus expands now in a momentum-conserving regime. During this second stage, the equation regulating the motion of the shell is

$$2\pi R_{\rm b}^2 H_{\rm eff} \rho_0 \dot{R}_{\rm b} = \frac{2L_{\rm w}}{v_{\rm w}} f(R_{\rm b}, H_{\rm eff})(t - t_{\rm br}) + \frac{\pi}{4}\frac{4\pi}{3}\left(\frac{H_{\rm eff}^7 L_{\rm w} \rho_0^2}{17.9}\right)^{1/3}. \tag{A3}$$

The term on the left hand side represents the shell momentum; the first term on the right hand side describes the wind momentum transferred to the shell after $t_{\rm br}$, while the second term indicates the shell momentum at $t_{\rm br}$[8]. This equation can be rewritten as

$$\dot{R}_{\rm b,2} = A \frac{f(R_{\rm b}, H_{\rm eff})}{R_{\rm b,2}^2}(t_6 - t_{\rm br,6}) + \frac{B}{R_{\rm b,2}^2}, \tag{A4}$$

where lengths are in 0.1 kpc and times in Myr. The two constants are

$$A = 35.23 \frac{L_{41}}{n_0 V_8}, \tag{A5}$$

and

$$B = 2.09 \left(\frac{H_{\rm eff,2}^4 L_{41}}{n_0}\right)^{1/3}, \tag{A6}$$

where $V_8 \equiv V_{\rm w}/(10^8\ {\rm cm\ s^{-1}})$, and $f(R_{\rm b}, H_{\rm eff})$ is a geometrical factor evaluating the fraction of the total wind momentum in the plane which is transferred to the shell:

$$f(\theta) = \int_\theta^{\pi/2} \sin(\alpha)^2 {\rm d}\alpha = 0.25\,(\pi - 2\theta + \sin(2\theta))\,, \tag{A7}$$

where α is the angle between the normal to the plane and the radial wind velocity direction, and $\theta = \arctan(R_{\rm b}/H)$[9].

Equation (A4) can be integrated numerically. However, we find an excellent analytical approximation (with a percentage error rarely above 3%, and never higher than 6%) to the numerical solution:

$$R(t)_{\rm b,2} = H_{\rm eff,2} \left(\frac{t}{t_{\rm br}}\right)^{\beta}; \tag{A8}$$

the exponent β can be very well approximated by

$$\beta = \mathcal{C} \left(\frac{\mathcal{L}}{0.01}\right)^{\gamma}, \tag{A9}$$

where $\mathcal{L} \equiv L_{41}/n_0$. The constant $\mathcal{C}$ depends on $H_{\rm eff}$: $\mathcal{C} = 0.421$ for $H_{\rm eff,2} = 1$, and $\mathcal{C} = 0.397$ for $H_{\rm eff,2} = 2$. For $0.01 \le \mathcal{L} \le 1$ it is $\gamma = 0.039$ for both the values of $H_{\rm eff}$; instead, if $0.001 \le \mathcal{L} < 0.01$, it is $\gamma = 0.034$ for $H_{\rm eff,2} = 1$, and $\gamma = 0.017$ for $H_{\rm eff,2} = 2$.

Equation (A8) holds up to $t_{\rm SN}$, the time at which the SNe II stop to explode. At later times, however, the shell may still keep expanding due to its "inertia". Such an expansion is regulated by an equation similar to equation A3, but without the contribution of the wind momentum [10]

$$R_{\rm b}^2(t)\dot{R}_{\rm b}(t) = R_{\rm b}^2(t_{\rm SN})\dot{R}_{\rm b}(t_{\rm SN}). \tag{A10}$$

The above equation can be easily solved, and one obtains the time evolution of the shell radius during this third stage:

$$R_{\rm b,2}(t) = \left(3\beta \frac{R_{\rm b,2}^3(t_{\rm SN,6})}{t_{\rm SN,6}}(t_6 - t_{\rm SN,6}) + R_{\rm b,2}^3(t_{\rm SN,6})\right)^{1/3}. \tag{A11}$$

In conclusion, we can summarize the evolution of the hole expansion as

[8] Koo & McKee (1992) considered only the shell momentum term; in fact, in their case, the first term is negligible because of the relatively low values of $L_{\rm w}$ considered.

[9] At the end of the first stage it is $\theta \sim 0$, and $f(0) = \pi/4$; this explains the presence of such numerical coefficient in the second term in the right end side of equation (A3).

[10] During this stage, as during the previous ones, we neglect the ISM pressure during the bubble expansion. The outward progress of the shell is thus maintained by the momentum of the outward moving gas (Spitzer 1978). The expansion stops at the dissolution of the shell occurring when the shell velocity is about σ_0.

$$R_{\rm b,2}(t_6) = \begin{cases} 2.7\mathcal{L}^{1/5} t_6^{3/5} & \text{if } t \le t_{\rm br} \\ H_{\rm eff,2} \left(\frac{t}{t_{\rm br}}\right)^{\beta} & \text{if } t_{\rm br} < t \le t_{\rm SN} \\ (3\beta \frac{R^3_{\rm b,2}(t_{\rm SN,6})}{t_{\rm SN,6}} (t_6 - t_{\rm SN,6}) + & \\ + R^3_{\rm b,2}(t_{\rm SN,6}))^{1/3} & \text{if } t > t_{\rm SN} \end{cases}$$

In the above equation we made use of the parameter $\mathcal{L}$ introduced earlier. In fact, the wind luminosity and the density of the ambient medium never occur separately in the equations, but always as a ratio. Therefore the hole expansion is regulated only by two parameters: $\mathcal{L}$ and, to a lesser extent, $H_{\rm eff}$.

This paper has been typeset from a TEX/LATEX file prepared by the author.